

One-loop electroweak radiative corrections to polarized $e^+e^- \rightarrow \gamma Z$ process

S. Bondarenko¹, Ya. Dydyshka^{2,3}, L. Kalinovskaya², L. Rumyantsev²,
R. Sadykov², and V. Yermolchuk^{2,3}

¹Bogoliubov Laboratory of Theoretical Physics, JINR, 141980 Dubna, Moscow region, Russia

²Dzhelepov Laboratory of Nuclear Problems, JINR, 141980 Dubna, Moscow region, Russia

³Institute for Nuclear Problems, Belarusian State University, Minsk, 220006 Belarus

November 24, 2021

Abstract

This paper gives high-precision theoretical predictions for cross sections of the process $e^+e^- \rightarrow \gamma Z$ for future electron-positron colliders. The calculations are performed using the **SANC** system. They include complete one-loop electroweak radiative corrections, as well as longitudinal polarization of initial state. The analytic expressions for covariant and helicity amplitudes are presented. Numerical results are given for the center-of-mass energy range $\sqrt{s} = 250 - 1000$ GeV with various polarization degrees. The influence of the kinematic setup and choice of electroweak schemes are also discussed.

1 Introduction

The physical programs at future e^+e^- colliders are developed to be complementary and synergistic with future hadron colliders.

Clean experimental conditions, negligible pile-up and controllable centre-of-mass energy, part-per-mil accuracy for cross sections for signal and background processes, well understood backgrounds for final states, allow to scan for new physics by precise measurement of deviations from the Standard Model [1, 2].

For direct observation of such a new physics the 100 TeV hadron collider is needed. But there are challenges that arise from the very richness of the e^+e^- program. One needs to match the theoretical accuracy to the statistical one, by taking into account electroweak (EW) radiative corrections (RCs) [3]. Polarized beams can improve opportunities for investigation of fundamental particles properties [2, 4–7].

Modern evaluation tools to estimate the theoretical uncertainties for future e^+e^- colliders, i.e. FCCee [6], ILC [8], CLIC [9], CEPC [9] should be applied.

We continue to develop the **SANC** system [6, 10, 11] in e^+e^- mode. Our experience in estimating the contribution of polarization effects for cross sections of $e^+e^- \rightarrow e^+e^-(HZ, \mu^+\mu^-, \tau^+\tau^-)$ processes was given in papers [12–14] for energies of the future e^+e^- colliders.

In this article we revised the uncertainties in theoretical interpretation for the process [15]

$$e^+(p_1, \chi_1) + e^-(p_2, \chi_2) \rightarrow \gamma(p_3, \chi_3) + Z(p_4, \chi_4) \quad (1)$$

at the complete one-loop electroweak level and evaluated the effects due to longitudinal polarization. We keep all masses in the one-loop calculation and work in full phase space.

First of all, this process is of particular interest to study the anomalous neutral tri-linear $Z\gamma V$, ($V = \gamma, Z$) gauge couplings. This kind of research was carried out by several working groups on anomalous gauge boson interactions in [16–21]. The constraints on these couplings are investigated at electron-positron collider through the γZ production of the final Z boson polarization states.

Secondly, this process and the process $e^+e^- \rightarrow ZZ$ are the main background for the reaction $e^+e^- \rightarrow ZH$ at 250 GeV in the Higgs boson measurements method. This method should identify Higgs boson events independently of the decay mode, allowing the measurement of the total cross section for Higgs production. The reaction $e^+e^- \rightarrow ZZ$ will be studied in the future.

One-loop QED and EW corrections to the unpolarized $e^+e^- \rightarrow \gamma Z$ process were previously calculated in the papers [16, 17, 19, 22]. However, it is difficult to draw a direct comparison between our results and these papers due to incomplete setups. The transverse beam polarization for this reaction was earlier considered in paper [21].

All calculations were done via the **MCSANCe** [23] integrator and **ReneSANCe** generator [24].

We discuss the covariant and tensor structures and present them in a compact form. The helicity amplitude (HA) approach and their expressions are given for the virtual part. The contribution of the hard real photon emission is obtained by direct squaring of the matrix element.

Numerical results are presented for the total and differential cross sections, which are the functions of the cosine of the scattering angle $\cos\vartheta_Z$, and for relative corrections in $\alpha(0)$ and G_μ EW schemes. They are completed with an estimation of polarization effects. The comparisons of our results at tree level for the Born and hard photon bremsstrahlung with **CalcHEP** [25] and **WHIZARD** [26, 27] are also given.

Having in the final state of the $e^+e^- \rightarrow \gamma Z \gamma$ reaction two identical photons, the different angular and energy cuts can be used in the analysis which depend on the kinematics of event selection criteria.

The article is organized as follows. Section 2 describes the general approach of the implementation of polarization effects into **SANC**. We present a compact form for the expressions for covariant (CA) and helicity amplitudes for Born, virtual and soft photon bremsstrahlung contributions. In Section 3 the corresponding numerical results are given for total and differential cross sections as well as for relative corrections. Numerical results are completed with an estimation of polarization effects. The left-right asymmetry is also considered. In Section 4 we analyze the results and discuss possible further improvements for this process in **SANC**.

2 Differential cross section

To study the case of the longitudinal polarization with degrees P_{e+} and P_{e-} , we produce helicity amplitudes and make a formal application of Eq. (1.15) from [4]:

$$\sigma(P_{e+}, P_{e-}) = \frac{1}{4} \sum_{\chi_1, \chi_2} (1 + \chi_1 P_{e+})(1 + \chi_2 P_{e-}) \sigma_{\chi_1 \chi_2}, \quad (2)$$

where $\chi_{1(2)} = -1(+1)$ corresponds to the particle i with the left (right) helicity.

The cross section of the process at one-loop level can be divided into four parts:

$$\sigma^{\text{one-loop}} = \sigma^{\text{Born}} + \sigma^{\text{virt}}(\lambda) + \sigma^{\text{soft}}(\lambda, \bar{\omega}) + \sigma^{\text{hard}}(\bar{\omega}),$$

where σ^{Born} is the Born cross section, σ^{virt} is the contribution of virtual(loop) corrections, σ^{soft} is the contribution of soft photon emission, σ^{hard} is the contribution of hard photon emission (with energy $E_\gamma > \bar{\omega}$). Auxiliary parameters λ ("photon mass") and $\bar{\omega}$ (soft-hard separator) are canceled after summation.

The virtual (Born) cross section of the $e^+e^- \rightarrow \gamma Z$ process can be written as follows:

$$\frac{d\sigma_{\chi_1 \chi_2}^{\text{virt(Born)}}}{d \cos \vartheta_\gamma} = \frac{\pi \alpha^2}{2c_W^2 s_W^2} \frac{s - M_Z^2}{s^2} |\mathcal{H}_{\chi_1 \chi_2}^{\text{virt(Born)}}|^2, \quad (3)$$

where

$$|\mathcal{H}_{\chi_1 \chi_2}^{\text{virt(Born)}}|^2 = \sum_{\chi_3, \chi_4} |\mathcal{H}_{\chi_1 \chi_2 \chi_3 \chi_4}^{\text{virt(Born)}}|^2, \quad (4)$$

final photon γ .

2.1 Covariant amplitude for Born and virtual part

In this section we continue the presentation of formulae for the amplitudes of process started in Section 2 of Ref. [15]. As usual, we begin with the calculation of CA corresponding to a result of the straightforward computation of *all* diagrams contributing to a given process at the one-loop level. It is represented in a certain *basis of structures*, made of strings of Dirac matrices and external momenta, contracted with polarization vectors of vector bosons. The amplitude is parameterized by a number of form factors (FFs), which we denote by \mathcal{F} , with an index labeling the corresponding structure. Number of FFs is by construction equal to the number of structures, however for cases presented below, some of the FFs can be equal to each other, and the number of independent FFs may be less than the number of structures. For existing tree level structures the corresponding FFs have the following form

$$\mathcal{F} = 1 + \frac{\alpha}{4\pi s_W^2} \tilde{\mathcal{F}}, \quad (5)$$

where "1" is due to the Born level and $\tilde{\mathcal{F}}$ is due to the one-loop level. As usual, we use various coupling constants:

$$Q_e, \quad I_e^{(3)}, \quad \sigma_e = v_e + a_e, \quad \delta_e = v_e - a_e, \quad s_W = \frac{e}{g}, \quad c_W = \frac{M_W}{M_Z}, \quad etc. \quad (6)$$

Given a CA, **SANC** computes a set of HAs, denoted by $\mathcal{H}_{\lambda_1\lambda_2\lambda_3\dots}$, where $\lambda_1\lambda_2\lambda_3\dots$ are the signs of particle spin projections onto a quantization axis.

The CA of the process $e^+e^- \rightarrow \gamma Z$ can be represented as a combination of 28 transversal in photonic 4-momentum structures and 14 vector \mathcal{F}_{vj} and 14 axial \mathcal{F}_{aj} form factors:

$$\mathcal{A} = \bar{v}(p_1) \left[\text{Str}_{\mu\nu}^0 (v_e \mathcal{F}_v^0 + a_e \gamma_5 \mathcal{F}_a^0) + \sum_{j=1}^{13} \text{Str}_{\mu\nu}^j (\mathcal{F}_v^j + \gamma_5 \mathcal{F}_a^j) \right] u(p_2) \varepsilon_\nu^\gamma(p_3) \varepsilon_\mu^Z(p_4), \quad (7)$$

$$\begin{aligned} \text{Str}_{\mu\nu}^0 &= i \left[\frac{1}{2} \left(\frac{1}{k_u} + \frac{1}{k_t} \right) \gamma_\mu \not{p}_3 \gamma_\nu + \frac{1}{k_u} (\not{p}_3 \delta_{\mu\nu} - \gamma_\nu p_{3\mu}) - \left(\frac{1}{k_u} p_{1\nu} - \frac{1}{k_t} p_{2\nu} \right) \gamma_\mu \right], \\ \text{Str}_{\mu\nu}^1 &= i \gamma_\mu \not{p}_3 \gamma_\nu, \text{Str}_{\mu\nu}^2 = \not{p}_3 \gamma_\nu p_{1\mu}, \text{Str}_{\mu\nu}^4 = \gamma_\mu \left(\not{p}_3 p_{1\nu} - \frac{1}{2} k_u \gamma_\nu \right), \\ \text{Str}_{\mu\nu}^6 &= i \left(\not{p}_3 p_{1\nu} - \frac{1}{2} k_u \gamma_\nu \right) p_{1\mu}, \text{Str}_{\mu\nu}^8 = i \left(\not{p}_3 p_{1\nu} - \frac{1}{2} k_u \gamma_\nu \right) p_{2\mu}, \\ \text{Str}_{\mu\nu}^{10} &= i (\not{p}_3 \delta_{\mu\nu} - \gamma_\nu p_{3\mu}), \text{Str}_{\mu\nu}^{11} = i \gamma_\mu [k_t p_{1\nu} - k_u p_{2\nu}], \\ \text{Str}_{\mu\nu}^{12} &= p_{1\mu} p_{2\nu} + p_{2\mu} p_{1\nu} + \frac{1}{2} k_t \delta_{\mu\nu}, \text{Str}_{\mu\nu}^{13} = [k_t p_{1\nu} - k_u p_{2\nu}] p_{2\mu}. \end{aligned} \quad (8)$$

Here the following notations are introduced: $\bar{v}(p_1)$, $u(p_2)$ and m_e are the bispinors and the mass of external fermions, respectively; $\varepsilon_\nu^\gamma(p_3)$ denotes the photon polarization vector and $\varepsilon_\mu^Z(p_4)$ denotes the Z boson polarization vector.

We also introduced quantities $k_i = m_e^2 - I$, $I = t, u$ with Mandelstam variables t and u

$$t = m_e^2 - Z_2(m_e), \quad u = m_e^2 - Z_1(m_e). \quad (9)$$

and

$$Z_1(m_e) = \frac{1}{2} Z_4(M_Z) (1 + \beta \cos \vartheta_\gamma), \quad Z_2(m_e) = \frac{1}{2} Z_4(M_Z) (1 - \beta \cos \vartheta_\gamma), \quad (10)$$

$$Z_4(M_Z) = s - M_Z^2, \quad \beta = \sqrt{1 - 4m_e^2/s}. \quad (11)$$

In Eq. (7) we keep the fermion mass in order to maintain photon transversality. Moreover in mass-containing denominators of Str^0 , the mass cannot be neglected because these denominators correspond to propagators of fermions which emit external photons and thus would lead to mass singularities.

The structures $\text{Str}_{\mu\nu}^{3,5,7,9}$ can be obtained from the structures $\text{Str}_{\mu\nu}^{2,4,6,8}$ by replacing $p_{1j} \rightarrow p_{2j}, u \rightarrow t$.

2.2 Helicity amplitudes for Born and virtual part

As it was shown in [16] all one-loop corrections for this process are symmetric at $u \leftrightarrow t$ exchange, so that there is no forward-backward asymmetry, which could be easier

observed without polarization. There are 24 nonzero HAs for the virtual contribution:

$$\begin{aligned}
\mathcal{H}_{\mp\mp\mp\mp} &= \frac{m_e}{\sqrt{s}} \left[2 - \frac{1}{2} \frac{sk_{tu}}{Z_1(m_e)Z_2(m_e)} \sin^2 \theta_\gamma \right] v_e \mathcal{F}_v^0 \\
&\quad + \frac{k_{tu}}{4\sqrt{s}} c_- \left[c_+ (\mathcal{F}_2^\pm - \mathcal{F}_3^\pm - \mathcal{F}_4^\pm) - c_- \mathcal{F}_5^\pm + \mathcal{F}_{12}^\pm - \frac{s}{2} c_+ \mathcal{F}_{13}^\pm \right], \\
\mathcal{H}_{\mp\mp\mp 0} &= \mp \frac{k_{tu}}{4\sqrt{2}M_Z} \sin \theta_\gamma \left[\frac{4M_Z^2 m_e}{Z_1(m_e)Z_2(m_e)} \cos \theta_\gamma v_e \mathcal{F}_v^0 \right. \\
&\quad \left. + k_2 \mathcal{F}_2^\pm + k_1 \mathcal{F}_3^\pm - k_2 \mathcal{F}_4^\pm + k_+ c_- \mathcal{F}_5^\pm - s \mathcal{F}_{12}^\pm + \frac{s}{2} k_1 \mathcal{F}_{13}^\pm \right], \\
\mathcal{H}_{\mp\mp\mp\pm} &= \frac{\sqrt{s}}{4} k_{tu} \sin^2 \theta_\gamma \left[\frac{2m_e}{Z_1(m_e)Z_2(m_e)} v_e \mathcal{F}_v^0 - \mathcal{F}_2^\pm + \mathcal{F}_3^\pm + \mathcal{F}_4^\pm - \mathcal{F}_5^\pm + \frac{s}{2} \mathcal{F}_{13}^\pm \right], \\
\mathcal{H}_{\mp\mp\pm\mp} &= \frac{\sqrt{s}}{8} k_{tu} \sin^2 \theta_\gamma \left[\frac{4m_e}{Z_1(m_e)Z_2(m_e)} v_e \mathcal{F}_v^0 + s \mathcal{F}_{13}^\pm \right], \\
\mathcal{H}_{\mp\mp\pm 0} &= \pm \frac{k_{tu}}{\sqrt{2}M_Z} \sin \theta_\gamma \left[\frac{m_e}{Z_1(m_e)Z_2(m_e)} (M_Z^2 \cos \theta_\gamma v_e \mathcal{F}_v^0 \pm k_{tu} a_e \mathcal{F}_a^0) \right. \\
&\quad \left. - \frac{s}{4} (2\mathcal{F}_4^\pm + \mathcal{F}_{12}^\pm - \frac{1}{2} k_1 \mathcal{F}_{13}^\pm) \right], \\
\mathcal{H}_{\mp\mp\pm\pm} &= \frac{m_e}{2\sqrt{s}} \left[\left(4 - (2k_{tu} + s \sin^2 \theta_\gamma) \frac{k_{tu}}{Z_1(m_e)Z_2(m_e)} \right) v_e \mathcal{F}_v^0 \right. \\
&\quad \left. \pm 2 \frac{Z_4^2(M_Z)}{Z_1(m_e)Z_2(m_e)} \cos \theta_\gamma a_e \mathcal{F}_a^0 \right] \\
&\quad - \frac{\sqrt{s}}{2} k_{tu} \left(c_+ \mathcal{F}_4^\pm - \frac{1}{2} c_- \mathcal{F}_{12}^\pm + \frac{s}{4} \sin^2 \theta_\gamma \mathcal{F}_{13}^\pm \right), \\
\mathcal{H}_{\pm\mp\pm\pm} &= \mp \frac{1}{8} \sin \theta_\gamma \left[\frac{4M_Z^2}{Z_1(m_e)} \mathcal{F}_0^\pm - k_{tu} [sc_+ (\mathcal{F}_6^\pm - \mathcal{F}_8^\pm) + 4\mathcal{F}_{10}^\pm + 2sc_- \mathcal{F}_{11}^\pm] \right], \\
\mathcal{H}_{\pm\mp\mp\mp} &= \pm \frac{1}{8} \sin \theta_\gamma \left[\frac{4M_Z^2}{Z_2(m_e)} \mathcal{F}_0^\pm \right. \\
&\quad \left. - k_{tu} [8\mathcal{F}_1^\pm + sc_- (\mathcal{F}_7^\pm - \mathcal{F}_9^\pm) - 4\mathcal{F}_{10}^\pm + 2sc_+ \mathcal{F}_{11}^\pm] \right], \\
\mathcal{H}_{\pm\mp\pm 0} &= \frac{1}{8\sqrt{2}} \frac{\sqrt{s}}{M_Z} c_+ \left[\frac{8M_Z^2}{Z_1(m_e)} \mathcal{F}_0^\pm + k_{tu} (k_2 \mathcal{F}_6^\pm + k_1 \mathcal{F}_8^\pm - 4\mathcal{F}_{10}^\pm - 2k_+ c_- \mathcal{F}_{11}^\pm) \right], \\
\mathcal{H}_{\mp\pm\pm 0} &= \frac{1}{8\sqrt{2}} \frac{\sqrt{s}}{M_Z} c_- \left[\frac{-8M_Z^2}{Z_2(m_e)} \mathcal{F}_0^\pm \right. \\
&\quad \left. + k_{tu} (8\mathcal{F}_1^\pm + k_2 \mathcal{F}_7^\pm + k_1 \mathcal{F}_9^\pm - 4\mathcal{F}_{10}^\pm + 2k_+ c_+ \mathcal{F}_{11}^\pm) \right], \\
\mathcal{H}_{\pm\mp\pm\mp} &= \mp \frac{s}{8} k_{tu} \sin \theta_\gamma c_+ \left[\frac{2}{Z_1(m_e)Z_2(m_e)} \mathcal{F}_0^\pm + \mathcal{F}_6^\pm - \mathcal{F}_8^\pm - 2\mathcal{F}_{11}^\pm \right], \\
\mathcal{H}_{\pm\mp\mp\pm} &= \pm \frac{s}{8} k_{tu} \sin \theta_\gamma c_- \left[\frac{2}{Z_1(m_e)Z_2(m_e)} \mathcal{F}_0^\pm + \mathcal{F}_7^\pm - \mathcal{F}_9^\pm - 2\mathcal{F}_{11}^\pm \right]. \tag{12}
\end{aligned}$$

Here we introduce the following shorthand notation

$$\begin{aligned}\mathcal{F}_0^\pm &= v_e \mathcal{F}_v^0(s, t, u) \pm a_e \mathcal{F}_a^0(s, t, u), \\ \mathcal{F}_j^\pm &= \mathcal{F}_v^j(s, t, u) \pm \mathcal{F}_a^j(s, t, u), \quad j = 1, \dots, 13, \\ k_{1,2} &= s c_\pm - M_Z^2 c_\mp, \quad c_\pm = 1 \pm \cos \vartheta_\gamma, \quad k_{tu} = t + u,\end{aligned}\tag{13}$$

The form factors should be set to $\mathcal{F}_0^\pm = 1$ and all others to zero in order to get Born HAs.

2.3 Soft and hard bremsstrahlung contributions

The bremsstrahlung module of the **SANC** system computes the contributions due to soft and inclusive hard real photon emission. The soft photon contribution contains infrared divergences and has to compensate the corresponding divergences of one-loop virtual QED corrections. The soft photon bremsstrahlung correction can be calculated analytically. It is factorized in front of the Born cross section. It depends on the auxiliary parameter which separates kinematical domains of soft and hard photon emission in a given reference frame. The polarization dependence is contained in σ^{Born} . The explicit form for soft photon contribution is

$$\sigma^{\text{soft}} = \sigma^{\text{Born}} \frac{\alpha}{2\pi} Q_e^2 \left\{ -L_s^2 + 4 \ln \frac{2\bar{\omega}}{\lambda} L_s - \frac{2\pi^2}{3} + 1 \right\}.\tag{14}$$

Here $\bar{\omega}$ is the soft-hard separator, λ is an auxiliary infinitesimal photon mass, and $L_s = \ln \frac{s}{m_e^2} - 1$.

The contribution of the hard real photon emission is obtained by direct squaring of the matrix element. Explicit formulas for differential distribution of the $e^+e^- \rightarrow \gamma Z \gamma$ process with one hard photon emission are too long to be listed here.

3 Numerical results and comparisons

In this Section, we present numerical results for the EW RCs to $e^+e^- \rightarrow \gamma Z$ process at one-loop level. Numerical results are completed by estimating of the polarization effect and evaluating angular and energy distributions in two EW schemes $\alpha(0)$ and G_μ . The c.m. energy set is $\sqrt{s} = 250, 500$ and 1000 GeV. The unpolarized as well as fully longitudinally polarized states with the magnitudes of the positron (P_{e+}) and electron (P_{e-}) beam polarization

$$(P_{e+}, P_{e-}) = (0, 0), (-1, -1), (-1, +1), (+1, -1), (+1, +1)\tag{15}$$

are considered. It is very convenient to present the results for longitudinal polarization of electron and positron colliding beams when P_{e+} and P_{e-} are, respectively, equal to $+1$ for completely polarized right-handed beams and -1 for completely polarized left-handed beams. the set $\sigma_{--}, \sigma_{-+}, \sigma_{+-}$ and σ_{++} of cross sections.

Triple tuned comparisons of our results at the tree level with the ones existing in the literature (**CalcHEP** [25] and **WHIZARD** [26], [27]) are also given.

For numerical evaluations we used the following set of input parameters:

$$\begin{aligned}
\alpha(0) &= 1/137.03599976 & G_{\text{Fermi}} &= 1.16637 \times 10^{-5} \text{ GeV}^{-2}, \\
M_Z &= 91.1876 \text{ GeV}, & \Gamma_Z &= 2.49977 \text{ GeV}, \\
M_W &= 80.451495 \text{ GeV} & M_H &= 125.0 \text{ GeV}, \\
m_e &= 0.5109990 \text{ MeV}, & m_\mu &= 0.105658 \text{ GeV}, \\
m_\tau &= 1.77705 \text{ GeV}, & & \\
m_u &= 0.062 \text{ GeV}, & m_d &= 0.083 \text{ GeV}, \\
m_c &= 1.5 \text{ GeV}, & m_s &= 0.215 \text{ GeV}, \\
m_t &= 173.8 \text{ GeV}, & m_b &= 4.7 \text{ GeV}.
\end{aligned} \tag{16}$$

The angular and energy cuts are additionally discussed.

3.1 Triple comparison of the tree level results: Born and hard photon bremsstrahlung cross sections

P_{e^+}, P_{e^-}	-1, -1	-1, +1	+1, -1	+1, +1
$\sigma_{e^+e^-}^{\text{hard}}, \text{ pb}, \sqrt{s} = 250 \text{ GeV}$				
S	2.51(1)	69.74(1)	110.09(1)	2.53(1)
C	2.53(1)	69.75(1)	110.09(1)	2.53(1)
W	2.53(1)	69.75(1)	110.07(2)	2.53(1)
$\sigma_{e^+e^-}^{\text{hard}}, \text{ pb}, \sqrt{s} = 500 \text{ GeV}$				
S	0.74(1)	17.04(1)	26.89(1)	0.75(1)
C	0.76(1)	17.03(1)	26.88(1)	0.76(1)
W	0.76(1)	17.05(1)	26.90(1)	0.76(1)
$\sigma_{e^+e^-}^{\text{hard}}, \text{ pb}, \sqrt{s} = 1000 \text{ GeV}$				
S	0.202(1)	4.604(1)	7.266(1)	0.206(1)
C	0.206(1)	4.603(1)	7.267(1)	0.206(1)
W	0.206(1)	4.603(1)	7.265(1)	0.206(1)

Table 1: Tuned triple comparison between **SANC** (first line), **CalcHEP** (second line) and **WHIZARD** (third line) results for the hard bremsstrahlung contributions to polarized $e^+e^- \rightarrow \gamma Z(\gamma)$ scattering for various degrees of polarization and energies.

First of all, we present triple comparison of numerical results for fully polarized Born and hard photon bremsstrahlung cross sections with the ones obtained via **CalcHEP** [25] and **WHIZARD** [26], [27] codes. The integration was performed without any angular cuts.

The agreement for the Born cross section was found to be excellent (we omit corresponding table). Table 1 shows very good agreement between **SANC** results (the first row) for the hard photon bremsstrahlung cross section contributions, **CalcHEP** results (the second row) and **WHIZARD** results (the third row).

The results are given within the $\alpha(0)$ EW scheme for three c.m. energies $\sqrt{s}=250, 500$ and 1000 GeV , with any photon energy $E_\gamma \geq \bar{\omega}, \bar{\omega} = 10^{-4}\sqrt{s}/2$ and fixed 100% polarized initial beams in the full phase space.

3.2 Born, one-loop cross section and relative corrections

In this part of paper we give the results for Born, complete one-loop EW cross sections (in picobarns) as well as for relative corrections (in percent)

$$\delta = \frac{\sigma^{\text{one-loop}}}{\sigma^{\text{Born}}} - 1. \quad (17)$$

In the calculations following cuts were imposed:

- c.m. system angular cuts for the Born, soft and virtual contributions where there is only one photon in the final state $\cos \vartheta_\gamma \in [-0.9, 0.9]$ and for the hard contribution both photons must have a c.m. energy greater than $\bar{\omega}$;
- – Setup I: for the hard event to be accepted, $\cos \vartheta_Z$ and $\cos \vartheta_\gamma$ for the photon with highest energy must lie within the interval $[-0.9, 0.9]$;
- – Setup II: for the hard event to be accepted, $\cos \vartheta_Z$ and at least one photon $\cos \vartheta_{\gamma_1}, \cos \vartheta_{\gamma_2}$ must lie within the interval $[-0.9, 0.9]$.

It should be noted that Setup II coincide with the criteria which were used in [15].

3.2.1 Angular dependence

With polarized electron beams and the possibility to invert these polarization, four different polarized cross sections $\sigma_{--, -+, +-, ++}$ can be measured. We prefer to estimate 100% polarization and in this case the polarized cross sections is mainly determined by the components σ_{-+} and σ_{+-} .

Figures 1, 2 and 3 illustrate the angular dependence of the 100 % polarized cross sections (Born and one-loop level in the $\alpha(0)$ and G_μ EW schemes for Setup II (left panel) and the corresponding relative corrections for Setup I and Setup II (right panel), respectively at c.m. energies $\sqrt{s} = 250, 500$ and 1000 GeV. The ϑ_Z is the angle between the initial electron e^- and final Z -boson.

For all c.m. energies $\sqrt{s} = 250, 500$ and 1000 GeV the minimum of Born and one-loop cross sections are at zero while the maximum are at the cut value 0.9 of $\cos \vartheta_Z$. As seen from the left panels of the Figs. 1, 2 and 3 the one-loop cross sections are closer to each other than Born values for two $\alpha(0)$ and G_μ EW schemes.

At the zero value of $\cos \vartheta_Z$ there is no difference between the relative corrections δ for Setup I and Setup II for all energies. The influence of different setups becomes significant at $\cos \vartheta_Z = 0.2 - 0.25$. It should be also noted that the values of the δ decrease with increasing of the $\cos \vartheta_Z$ value. The decreasing becomes sharp after the value of $\cos \vartheta_Z = 0.8 - 0.85$.

Since there is a symmetry on the $\cos \vartheta_Z$ variable, differential cross sections only for $\cos \vartheta_Z \in [0, 0.9]$ are shown.

Hereinafter, for brevity, if the results for Setup I and Setup II are different, then the result for Setup I is shown first, and then for Setup II, in parentheses.

- The c.m. energy $\sqrt{s} = 250$ GeV

The magnitudes of relative corrections at $\cos \vartheta_Z = 0$ are approximately equal to $\delta_{-+}[\alpha(0)] = 24.3\%$ and $\delta_{-+}[G_\mu] = 18.4\%$. Relative corrections at $\cos \vartheta_Z = 0.9$ (at angular cut value) are approximately equal to $\delta_{-+}[\alpha(0)] = -6.8\%$ (3.5%) and $\delta_{-+}[G_\mu] = -12.5\%$ (-2.1%).

Relative corrections of the component $\delta_{+-}[\alpha(0)]$ are of the order 7.5% and $\delta_{+-}[G_\mu] = 1.9\%$ at the zero value of $\cos \vartheta_Z$. The value vary more slowly than δ_{+-} with increasing of the cosine: for $\alpha(0)$ EW scheme it is in the range between -21.8% (-11.5%) and at G_μ EW scheme in the range between -27.6% (-17.2%).

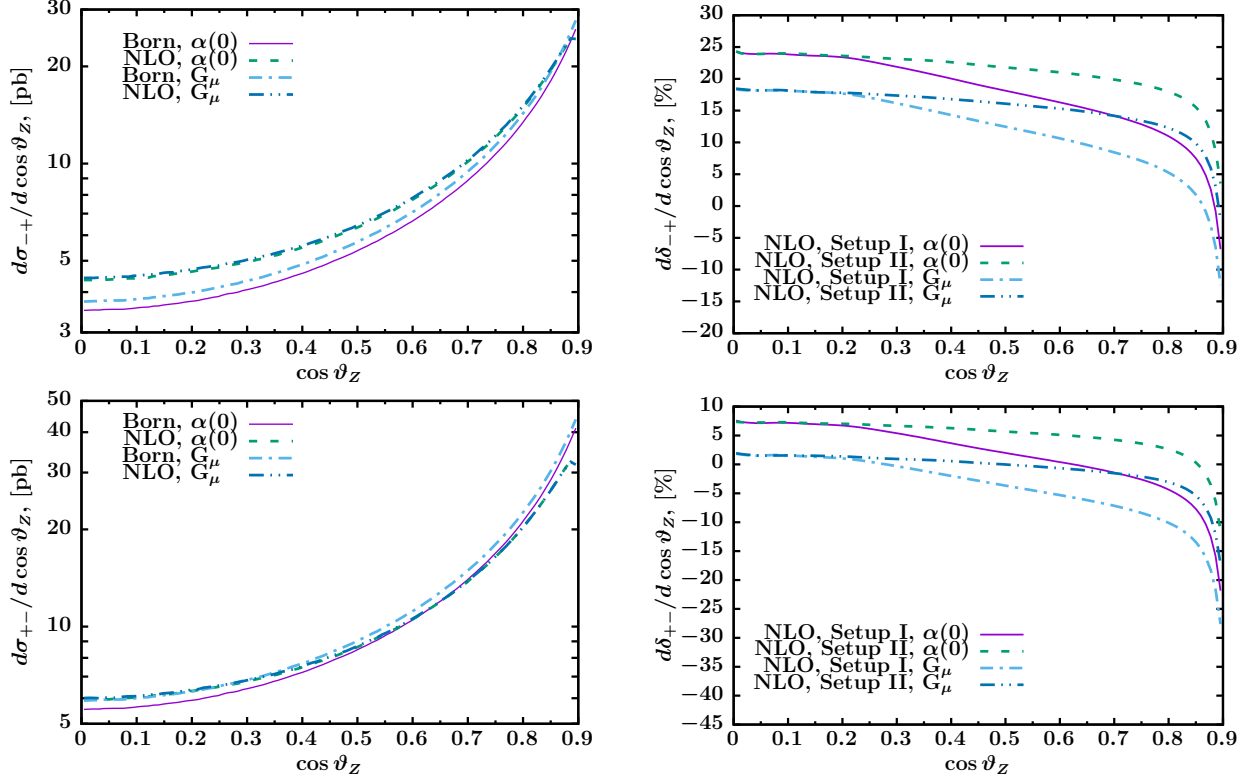


Figure 1: Polarized differential cross section [left, in pb, only Setup II] and relative corrections [right, in %] vs. the cosine of Z scattering angle at the c.m. energy $\sqrt{s} = 250$ GeV. Upper panel is for $(-+)$ and down is for $(+-)$ helicity configurations.

- The c.m. energy $\sqrt{s} = 500$ GeV

When considering the values of the cross section and the RCs at the c.m. energy $\sqrt{s} = 500$ GeV we see that their values decreases significantly with increasing energy.

Magnitude of the relative RCs for the component δ_{-+} at $\cos \vartheta_Z = 0$ are positive, and equal to 25% and tend to negative values with increasing of the $\cos \vartheta_Z$, reaching about -10.2% (1.7%) at $\cos \vartheta_Z = 0.9$ in the $\alpha(0)$ EW scheme.

In the G_μ EW scheme the behavior of the δ_{-+} is similar. Relative RCs are equal to 20% at the zero and decrease up to -15.8 % (-3.9%) at 0.9 value of $\cos \vartheta_Z$.

Relative corrections of the component δ_{+-} are of the order $\delta_{+-}[\alpha(0)] = -0.5\%$ and $\delta_{+-}[G_\mu] = -6\%$ at zero value of $\cos \vartheta_Z$ and rich up to $\delta_{+-}[\alpha(0)] = -27.9\%$ (-16.0%) and $\delta_{+-}[G_\mu] = -33.5\%$ (-21.7%) with increasing the cosine (till the cut value 0.9).

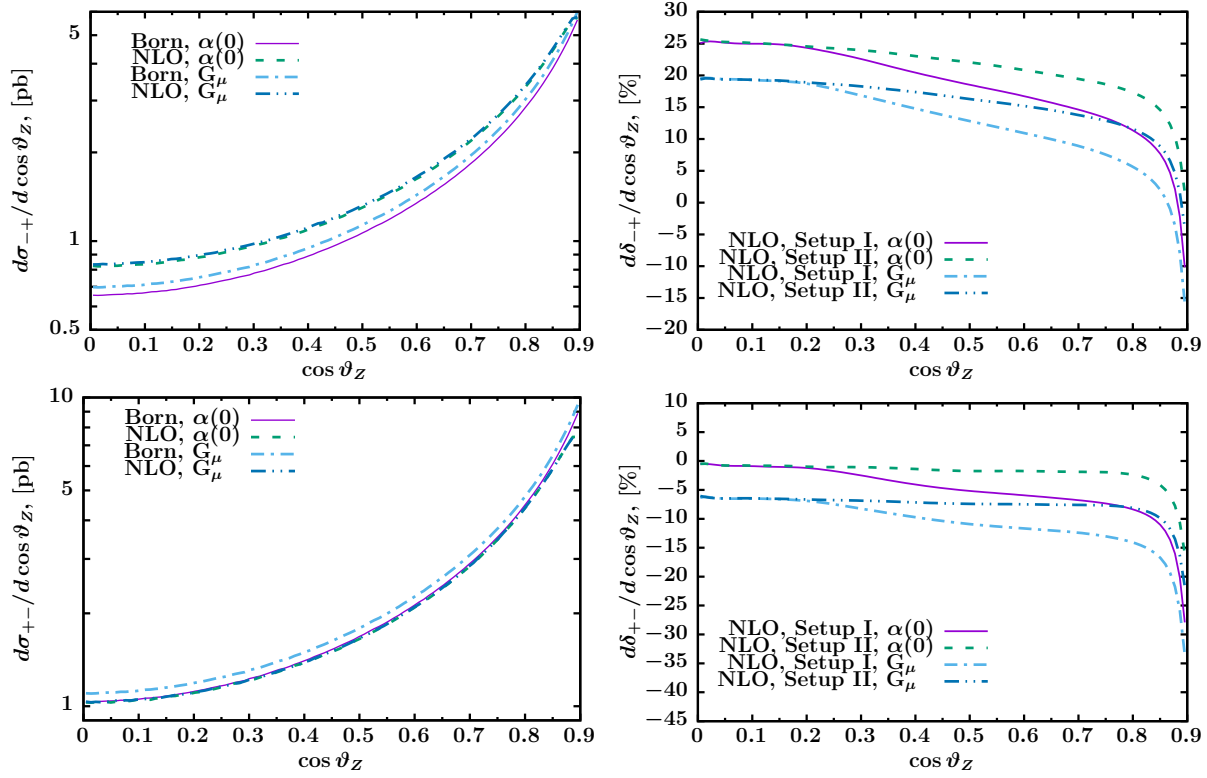


Figure 2: Polarized differential cross section [left, in pb, only Setup II] and relative corrections [right, in %] vs. the cosine of the Z scattering angle at the c.m. energy $\sqrt{s} = 500$ GeV. Upper panel is for $(-+)$ and down is for $(+-)$ helicity configurations.

- The c.m. energy $\sqrt{s} = 1000$ GeV

The $\delta_{-+}[\alpha(0)]$ is equal approximately 26% and $\delta_{-+}[G_\mu] = 20\%$ at $\cos \vartheta_Z = 0$. With increasing the cosine the value of $\delta_{-+}[\alpha(0)]$ riches -8.4% (0.27%) and $\delta_{-+}[G_\mu]$ -14.1% (-5.4%).

For the component δ_{+-} RCs are of the order -0.5% in $\alpha(0)$ and -6% in G_μ EW scheme at the zero value of the $\cos \vartheta_Z$. At $\cos \vartheta_Z = 0.9$ the relative correction δ_{+-} riches up to -27.9% (-16.0%) in the $\alpha(0)$ and -33.5% (-21.7%) in the G_μ EW schemes.

The magnitude of $\delta_{+-}[\alpha(0)]$ changes up to -32.7% (-24.2%) and of $\delta_{+-}[G_\mu]$ up to -38.5% (-29.9%) at $\cos \vartheta_Z = 0.9$.

3.2.2 Energy dependence

In Tables 2-4 the result of Born and one-loop cross sections, as well as relative corrections calculations of the $e^+e^- \rightarrow \gamma Z(\gamma)$ scattering for c.m. energies $\sqrt{s} = 250, 500$ and 1000 GeV in the $\alpha(0)$ and G_μ EW schemes are presented for Setup I and Setup II.

- The c.m. energy $\sqrt{s} = 250$ GeV

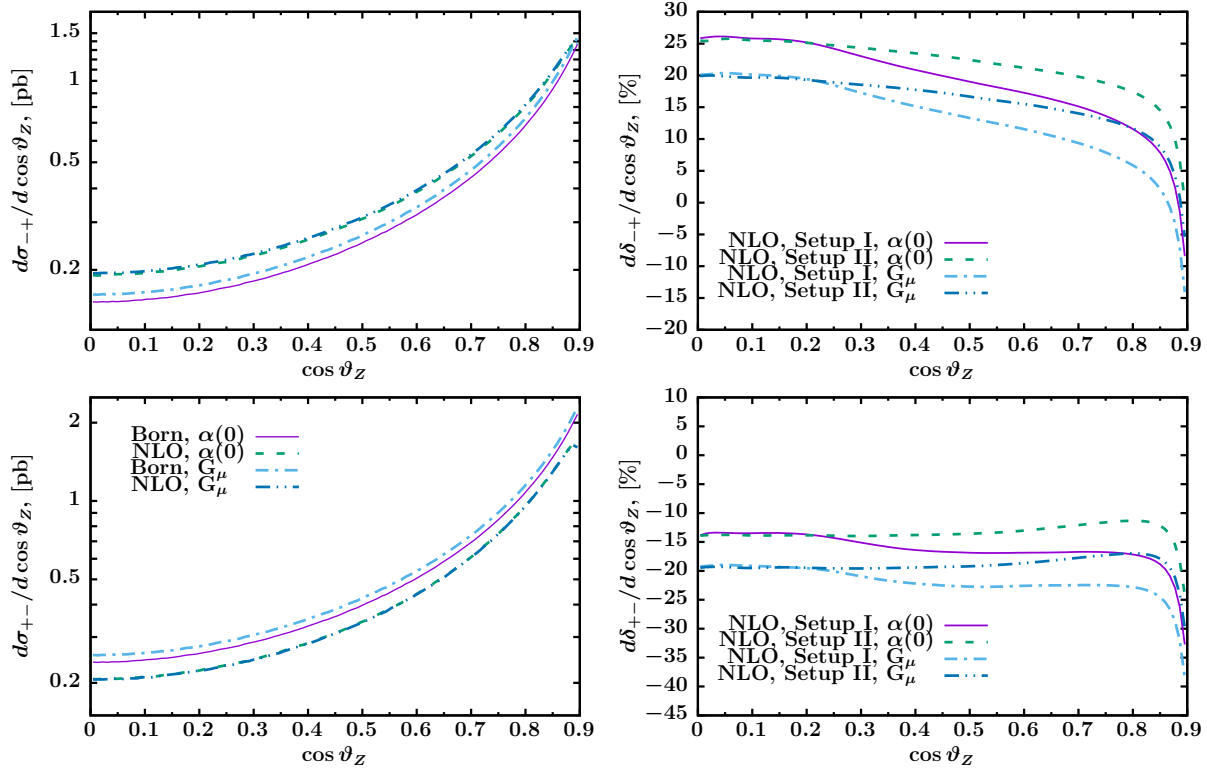


Figure 3: Polarized differential cross section [left, in pb, only Setup II] and relative corrections [right, in %] vs. the cosine of Z scattering angle at c.m. energy $\sqrt{s} = 1000$ GeV. Upper panel is for $(-+)$ and down is for $(+-)$ helicity configurations.

As seen, for the corrections for the unpolarized case in the $\alpha(0)$ EW scheme, the magnitudes δ are positive and equal to 4.6% (9.60%). The calculations in G_μ EW scheme reduce the magnitude of relative RCs to about 5-6 %, they become negative for Setup I and equal -1.16% and in the case of Setup II $\delta = 3.87\%$.

Relative RCs for the fully polarized case in the $\alpha(0)$ EW scheme are positive for δ_{-+} and are equal to 14.19% (19.19%), while relative correction δ_{+-} may change sign and become negative: $\delta_{+-}[\alpha(0)] = -1.62\%$ (3.38%). RCs in the G_μ are positive for δ_{-+} , i.e. 8.49% (13.48%) while the $\delta_{+-}[G_\mu]$ become negative -7.33% (-2.34%).

We observe a significant increase of RCs for Setup II compare to Setup I because the last one is more strong. It leads to a difference between relative corrections in Setup I and Setup II by about 5%.

- The c.m. energy $\sqrt{s} = 500$ GeV

The magnitude of relative RCs in the $\alpha(0)$ EW scheme for the unpolarized case are positive and equal to 0.92% (5.59%) while in G_μ EW scheme it is negative -4.77% (-0.12%).

Corresponding δ_{-+} in the $\alpha(0)$ EW scheme are positive and equal to 14.18% (18.79%). The relative RCs δ_{-+} in the G_μ EW scheme are positive: 8.47% (13.08%).

But for component $+-$ the RCs δ_{+-} change sign and become negative and reach about -7.53% (-2.92%) and -13.23% (-8.64%) correspondingly for $\alpha(0)$ and G_μ EW schemes.

- The c.m. energy $\sqrt{s} = 1000$ GeV,

P_{e^+}, P_{e^-}		0, 0	-1, -1	-1, +1	+1, -1	+1, +1
$\sigma_{\alpha(0)}^{\text{Born}}, \text{ pb}$		4.094(1)	—	6.3528(1)	10.025(1)	—
$\sigma_{\alpha(0)}^{\text{one-loop}}, \text{ pb}$	I	4.281(1)	0.0025(1)	7.254(1)	9.863(1)	0.0029(1)
	II	4.487(1)	0.0058(1)	7.572(1)	10.364(1)	0.0060(1)
$\delta_{\alpha(0)}, \%$	I	4.55(2)	—	14.19(1)	-1.62(1)	—
	II	9.60(2)	—	19.19(1)	3.38(1)	—
$\sigma_{G_\mu}^{\text{Born}}, \text{ pb}$		4.361(1)	—	6.7664(1)	10.678(1)	—
$\sigma_{G_\mu}^{\text{one-loop}}, \text{ pb}$	I	4.311(1)	0.0026(1)	7.341(1)	9.896(1)	0.0025(1)
	II	4.529(1)	0.0057(1)	7.679(1)	10.428(1)	0.0064(1)
$\delta_{G_\mu}, \%$	I	-1.16(2)	—	8.49(1)	-7.33(1)	—
	II	3.87(2)	—	13.48(1)	-2.34(1)	—

Table 2: Born and complete one-loop cross sections σ in pb, and relative corrections δ in % for the c.m. energy $\sqrt{s} = 250$ GeV, various polarization degrees of initial particles in $\alpha(0)$ and G_μ EW schemes and for Setup I and Setup II.

P_{e^+}, P_{e^-}		0, 0	-1, -1	-1, +1	+1, -1	+1, +1
$\sigma_{\alpha(0)}^{\text{Born}}, \text{ pb}$		0.8335(1)	—	1.2932(1)	2.0407(1)	—
$\sigma_{\alpha(0)}^{\text{one-loop}}, \text{ pb}$	I	0.8412(1)	0.00058(1)	1.4766(1)	1.8870(1)	0.00062(1)
	II	0.8801(1)	0.0017(1)	1.5362(1)	1.9811(1)	0.0014(1)
$\delta_{\alpha(0)}, \%$	I	0.92(2)	—	14.18(1)	-7.53(1)	—
	II	5.59(2)	—	18.79(1)	-2.92(1)	—
$\sigma_{G_\mu}^{\text{Born}}, \text{ pb}$		0.8878(1)	—	1.3774(1)	2.1736(1)	—
$\sigma_{G_\mu}^{\text{one-loop}}, \text{ pb}$	I	0.8453(3)	0.00063(1)	1.4940(1)	1.8859(3)	0.00082(1)
	II	0.8866(3)	0.0015(1)	1.5576(1)	1.9858(1)	0.0015(1)
$\delta_{G_\mu}, \%$	I	-4.77(2)	—	8.47(1)	-13.23(1)	—
	II	-0.12(2)	—	13.08(1)	-8.64(1)	—

Table 3: Born and complete one-loop cross sections σ in pb, and relative corrections δ in % for the c.m. energy $\sqrt{s} = 500$ GeV, various polarization degrees of initial particles in the $\alpha(0)$ and G_μ EW schemes and for Setup I and Setup II.

For c.m. energy $\sqrt{s}=1000$ GeV, we also observe quite marked difference between the results of the relative RCs δ in two EW schemes. The results in $\alpha(0)$ EW schemes are: for unpolarized case -5.02% (-0.66%), for $\delta_{-+} = 14.55\%$ (18.88%) and for $\delta_{+-} = -17.48\%$ (-13.17%); while in G_μ EW schemes: for Setup I (Setup II) -10.72% (-6.33%) for unpolarized case and for $\delta_{-+} = 8.85\%$ (13.16%) and for $\delta_{+-} = -23.20\%$ (-18.84%).

P_{e^+}, P_{e^-}		0, 0	-1, -1	-1, +1	+1, -1	+1, +1
$\sigma_{\alpha(0)}^{\text{Born}}, \text{ pb}$		0.1986(1)	—	0.30813(1)	0.48625(1)	—
$\sigma_{\alpha(0)}^{\text{one-loop}}, \text{ pb}$	I	0.18862(1)	0.00015(1)	0.35297(3)	0.4012(1)	0.00015(1)
	II	0.1973(1)	0.00034(1)	0.3663(1)	0.4222(1)	0.00032(1)
$\delta_{\alpha(0)}, \%$	I	-5.02(2)	—	14.55(1)	-17.48(1)	—
	II	-0.66(2)	—	18.88(1)	-13.17(1)	—
$\sigma_{G_\mu}^{\text{Born}}, \text{ pb}$		0.2115(1)	—	0.32819(1)	0.51790(1)	—
$\sigma_{G_\mu}^{\text{one-loop}}, \text{ pb}$	I	0.1888(1)	0.00016(1)	0.3572(1)	0.3978(1)	0.00017(1)
	II	0.1981(1)	0.00034(1)	0.3714(1)	0.4203(2)	0.00034(1)
$\delta_{G_\mu}, \%$	I	-10.72(2)	—	8.85(1)	-23.20(1)	—
	II	-6.33(2)	—	13.16(1)	-18.84(1)	—

Table 4: Born and complete one-loop cross sections σ in pb, and relative corrections δ in % for the c.m. energy $\sqrt{s} = 1000$ GeV, various polarization degrees of initial particles in $\alpha(0)$ and G_μ EW schemes and for Setup I and Setup II.

3.3 Left-right asymmetry

Fig. 4 shows the distributions of left-right asymmetry A_{LR} in $\cos \vartheta_Z$ for Born and one-loop contribution for c.m. energies $\sqrt{s} = 250, 500, 1000$ GeV in $\alpha(0)$ EW scheme and Setup II where A_{LR} is defined as follows:

$$A_{LR} = \frac{\sigma_{LR} - \sigma_{RL}}{\sigma_{LR} + \sigma_{RL}}, \quad (18)$$

with σ_{LR} and σ_{RL} are the cross sections for fully polarized electron-positron $e_L^- e_R^+$ and $e_R^- e_L^+$ initial states, correspondingly.

At Born level the A_{LR} is constant:

$$A_{LR}^{\text{Born}} = \frac{-3M_Z^4 + 4M_Z M_W}{5M_Z^4 - 12M_Z M_W + 8M_W^4} \approx 0.2243. \quad (19)$$

The asymmetry for c.m. energy $\sqrt{s} = 250$ GeV has rather flat behaviour while for 500 and 1000 GeV there is some increase at $\cos \vartheta_Z = 0.9$ value (the cut value) comparing to $\cos \vartheta_Z = 0$ value.

It should be emphasized that the dependence of A_{LR} on the EW scheme and setup choice is very weak.

4 Conclusion

In this paper we have described the evaluation of polarization effects for cross sections of the process $e^+ e^- \rightarrow \gamma Z$ at one-loop level at high energies for future $e^+ e^-$ colliders. The

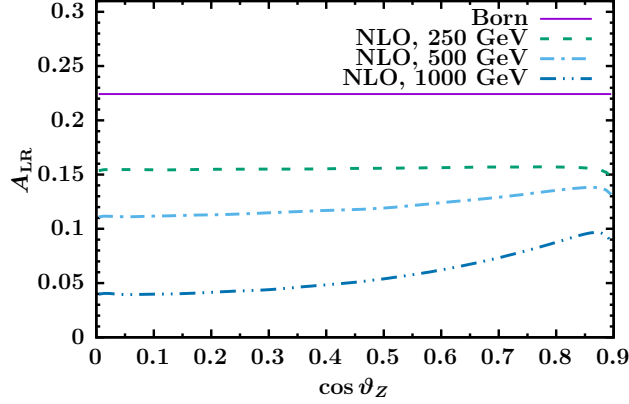


Figure 4: Distributions of left-right asymmetry A_{LR} in $\cos \vartheta_Z$ for Born and one-loop levels for c.m. energies $\sqrt{s} = 250, 500, 1000$ GeV in $\alpha(0)$ EW scheme and Setup II.

relevant contributions i.e. Born, virtual and real soft photon bremsstrahlung to the cross section were calculated analytically using the helicity amplitudes approach, which allows to evaluate the contributions of any longitudinal polarization and estimate them numerically. The hard photon bremsstrahlung contribution was obtained by direct squaring of the matrix element. All contributions have taken into account the initial particle masses. The effect of polarization of initial beams was carefully analyzed for certain states. The angular and energy dependencies for $\sigma_{--, --, +-, ++}$ were also considered.

The independence of the form factors of gauge parameters was tested, and the stability of the result on the variation of soft-hard separation parameter $\bar{\omega}$ was checked.

The calculated polarized tree-level cross sections for Born and hard photon bremsstrahlung were compared with CalcHEP and WHIZARD results and a very good agreement was found.

The polarization effects were found to be significant and the given increase in the cross section at definite initial degrees of polarization was compared to the unpolarized one. The radiative corrections themselves were rather sensitive to polarization degrees of initial beams and depended quite strongly on energy.

Two variants of experimental criteria (angular and energy cuts) were investigated. The difference in relative corrections was found to be about 5% between these setups.

Also the calculations in $\alpha(0)$ and G_μ EW schemes were considered. The results for relative corrections in G_μ EW scheme are approximately 5-6% less than in $\alpha(0)$ one. The difference between complete one-loop cross sections in considered EW schemes is about 1%. This could be considered as a theoretical uncertainty.

Combining the different experimental criteria, polarization degree of beams and EW schemes, radiative corrections could be minimized.

Considering the $e^+e^- \rightarrow \gamma Z$ process as main background of the reaction $e^+e^- \rightarrow ZH$ one needs to implement the decay modes ($e^+e^- \rightarrow \gamma f \bar{f}$, $e^+e^- \rightarrow Z f \bar{f}$, $e^+e^- \rightarrow 2f 2\bar{f}$) either in resonance approach for γ, Z decay or by the complete one-loop calculations.

Acknowledgments

This work has been supported by the RFBR grant 20-02-00441. We are grateful to Prof. A. Arbuzov for the help in preparation of the manuscript.

References

- [1] A. Blondel and P. Janot, 1809.10041.
- [2] A. Blondel, A. Freitas, J. Gluza, T. Riemann, S. Heinemeyer, S. Jadach, and P. Janot, 1901.02648.
- [3] L. The LEP Collaborations ALEPH, DELPHI, OPAL, and the LEP TGC Working Group.
- [4] G. Moortgat-Pick *et al.*, *Phys. Rept.* **460** (2008) 131–243, [hep-ph/0507011](#).
- [5] K. Fujii *et al.*, 1506.05992.
- [6] A. Blondel *et al.*, “Standard Model Theory for the FCC-ee: The Tera-Z”, in *Mini Workshop on Precision EW and QCD Calculations for the FCC Studies : Methods and Techniques CERN, Geneva, Switzerland, January 12-13, 2018*, 2018, 1809.01830.
- [7] P. Bambade *et al.*, 1903.01629.
- [8] ILC, ILC — <https://www.linearcollider.org/ILC>.
- [9] CLIC, CERN — clic-study.web.cern.ch/.
- [10] A. Andonov, A. Arbuzov, D. Bardin, S. Bondarenko, P. Christova, L. Kalinovskaya, G. Nanava, and W. von Schlippe, *Comput. Phys. Commun.* **174** (2006) 481–517, [Erratum: *Comput. Phys. Commun.* 177,623(2007)], [hep-ph/0411186](#).
- [11] A. Arbuzov, D. Bardin, S. Bondarenko, P. Christova, L. Kalinovskaya, U. Klein, V. Kolesnikov, L. Rumyantsev, R. Sadykov, and A. Saponov, *JETP Lett.* **103** (2016), no. 2 131–136, 1509.03052.
- [12] S. Bondarenko, Y. Dydyshka, L. Kalinovskaya, L. Rumyantsev, R. Sadykov, and V. Yermolchyk, *Phys. Rev. D* **100** (2019), no. 7 073002, 1812.10965.
- [13] S. Bondarenko, Y. Dydyshka, L. Kalinovskaya, R. Sadykov, and V. Yermolchyk, *Phys. Rev. D* **102** (2020), no. 3 033004, 2005.04748.
- [14] A. Arbuzov, S. Bondarenko, L. Kalinovskaya, R. Sadykov, and V. Yermolchyk, 2105.11708.
- [15] D. Bardin, S. Bondarenko, L. Kalinovskaya, G. Nanava, L. Rumyantsev, and W. von Schlippe, *Eur. Phys. J.* **C54** (2008) 187–197, 0710.3083.
- [16] M. Bohm and T. Sack, *Z. Phys.* **C35** (1987) 119.
- [17] F. A. Berends, G. J. H. Burgers, and W. L. van Neerven, *Phys. Lett.* **B177** (1986) 191–194.
- [18] H. Aihara *et al.*, “Anomalous gauge boson interactions”, in *Electroweak symmetry breaking and new physics at the TeV scale* (T. L. Barklow, S. Dawson, H. E. Haber, and J. L. Siegrist, eds.), 3, 1995, [hep-ph/9503425](#).

- [19] G. J. Gounaris, J. Layssac, and F. M. Renard, *Phys. Rev.* **D67** (2003) 013012, [hep-ph/0211327](#).
- [20] W. Hollik and C. Meier, *Phys. Lett.* **B590** (2004) 69–75, [hep-ph/0402281](#).
- [21] B. Ananthanarayan, S. D. Rindani, R. K. Singh, and A. Bartl, *Phys. Lett.* **B593** (2004) 95–104, [Erratum: *Phys. Lett.*B608,274(2005)], [hep-ph/0404106](#).
- [22] M. Capdequi Peyranere, Y. Loubatieres, and M. Talon, *Nuovo Cim.* **A90** (1985) 363.
- [23] A. B. Arbuzov *et al.*, *Comput. Phys. Commun.* (to be published) (2021).
- [24] R. Sadykov and V. Yermolchyk, *Computer Physics Communications* **256** (2020) 107445, [2001.10755](#).
- [25] A. Belyaev, N. D. Christensen, and A. Pukhov, *Comput. Phys. Commun.* **184** (2013) 1729–1769, [1207.6082](#).
- [26] W. Kilian, T. Ohl, and J. Reuter, *Eur. Phys. J.* **C71** (2011) 1742, [0708.4233](#).
- [27] W. Kilian, S. Brass, T. Ohl, J. Reuter, V. Rothe, P. Stienemeier, and M. Utsch, “New Developments in WHIZARD Version 2.6”, in *International Workshop on Future Linear Collider (LCWS2017) Strasbourg, France, October 23-27, 2017*, 2018, [1801.08034](#).